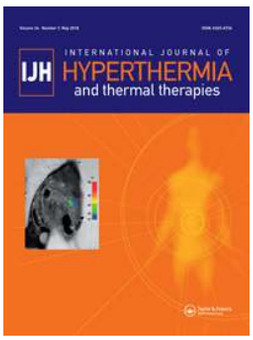

International Journal of Hyperthermia

ISSN: 0265-6736 (Print) 1464-5157 (Online) Journal homepage: https://www.tandfonline.com/loi/ihyt20

Non-Fourier thermal transport induced structural hierarchy and damage to collagen ultrastructure subjected to laser irradiation

Nilamani Sahoo, Arunn Narasimhan, Purbarun Dhar & Sarit K. Das

To cite this article: Nilamani Sahoo, Arunn Narasimhan, Purbarun Dhar & Sarit K. Das (2018) Non-Fourier thermal transport induced structural hierarchy and damage to collagen ultrastructure subjected to laser irradiation, International Journal of Hyperthermia, 34:3, 229-242, DOI: 10.1080/02656736.2017.1342873

To link to this article: https://doi.org/10.1080/02656736.2017.1342873

INTERNATIONAL JOURNAL OF HYPERTHERMIA, 2018
VOL. 34, NO. 3, 229–242
https://doi.org/10.1080/02656736.2017.1342873

Taylor & Francis
Taylor & Francis Group

Non-Fourier thermal transport induced structural hierarchy and damage to collagen ultrastructure subjected to laser irradiation

Nilamani Sahoo[a], Arunn Narasimhan[a], Purbarun Dhar[b] and Sarit K. Das[a]

[a]Department of Mechanical Engineering, Indian Institute of Technology Madras, Chennai, India; [b]Department of Mechanical Engineering, Indian Institute of Technology Ropar, Rupnagar, India

ABSTRACT

Comprehending the mechanism of thermal transport through biological tissues is an important factor for optimal ablation of cancerous tissues and minimising collateral tissue damage. The present study reports detailed mapping of the rise in internal temperature within the tissue mimics due to NIR (1064 nm) laser irradiation, both for bare mimics and with gold nanostructures infused. Gold nanostructures such as mesoflowers and nanospheres have been synthesised and used as photothermal converters to enhance the temperature rise, resulting in achieving the desired degradation of malignant tissue in targeted region. Thermal history was observed experimentally and simulated considering non-Fourier dual phase lag (DPL) model incorporated Pennes bio-heat transfer equation using COMSOL Multiphysics software. The gross deviation in temperature i.e. rise from the classical Fourier model for bio-heat conduction suggests additional effects of temperature rise on the secondary structures and morphological and physico-chemical changes to the collagen ultrastructures building the tissue mass. The observed thermal denaturation in the collagen fibril morphologies have been explained based on the physico-chemical structure of collagen and its response to thermal radiation. The large shift in frequency of amides A and B is pronounced at a depth of maximum temperature rise compared with other positions in tissue phantom. Observations for change in band of amide I, amide II, and amide III are found to be responsible for damage to collagen ultra-structure. Variation in the concentration of gold nanostructures shows the potentiality of localised hyperthermia treatment subjected to NIR radiation through a proposed free radical mechanism.

ARTICLE HISTORY
Received 25 January 2017
Revised 15 May 2017
Accepted 12 June 2017
Published online 7 July 2017

KEYWORDS
Collagen; laser; bio-heat transfer; hyperthermia; photo thermotherapy; structure; denaturation

Introduction

Application of lasers towards clinical diagnosis and photothermal therapy provides a new way for many researchers to focus on temperature history and intensity of damage to healthy tissues. The study of laser interaction with cancerous tissue to improve hyperthermia treatment efficacy depends on the electromagnetic spectrum. So the near infra-red (NIR) spectral region of 750–1100 nm shows the highest physiological transmission and is considered as a therapeutic window in clinical field [1]. The clinically well-established application of NIR spectrum is useful for the photothermal therapy of malignant tissues in the presence or the absence of plasmonic nanostructures and the resultant thermal damage history is an immensely important quantity to the oncosurgeons [2,3]. Such treatment needs to focus on accurate measurement of the complete thermal profile inside tissues and successive thermal damage to bio-tissues in the course of photothermal therapy. Researchers have approached to model the source term in bio-heat transfer equation by either Lambert's law or diffusion approximation. They numerically validated with the experimental temperature distribution results considering Fourier model of Pennes bio-heat equation [4–7]. Dai et al. [8] investigated theoretically to estimate the distribution of absorbed light in human skin. They developed a mathematical model composed with Monte Carlo algorithm, and numerical solution of bio-heat diffusion equation was used to calculate the transient temperature distribution, and a damage integral based on an empirical Arrhenius relationship to quantify the tissue damage. The bio-heat equation usually used for simulation considers an infinite propagation velocity for the heat wave. This explains that a change in the temperature at any part of the medium should disturb the temperature of a finite medium at each point instantaneously. But this theory is inappropriate towards microscopic approach of heat transfer analysis as bio-tissue contains many diverse chemical components. Nickel et al. [9] studied anisotropy of light propagation in human skin to observe a directional dependence i.e. steady-state diffuse reflectometry that helps for non-invasive diagnostic methods relying on skin optical properties. The anisotropic and heterogeneous nature of biological component makes the thermal signal to be propagated at a

CONTACT Sarit K. Das skdas@iitm.ac.in Department of Mechanical Engineering, Indian Institute of Technology Madras, Chennai 600036, India; Purbarun Dhar purbarun@iitrpr.ac.in Department of Mechanical Engineering, Indian Institute of Technology Ropar, Rupnagar, India

Supplemental data for this article can be accessed here.

finite speed. As a result, there is a delayed response between the heat flux vector and the temperature gradient.

However, in a bio-tissue, accumulating enough energy to transfer to the nearest particle takes time in the process of heat transfer. This finite time value (i.e. relaxation time) for materials with non-homogeneous inner structures has been questioned by Grabmann et al. [10] and Herwiget al. [11]. Both studies objected to the existence of hyperbolic conduction effect in materials with non-homogenous inner structures and proposed that classical Fourier model is more appropriate to predict the transient conduction behaviour in bio-tissue. To resolve these controversies, many research groups attempted to experimentally find out the relaxation time. Kaminski et al. [12] estimated the relaxation time for heat flux in the range of 20–30 s in material with non-homogeneous inner structures. Mitra et al. [13] also observed the evidence of non-Fourier behaviour with the processed meat and found the relaxation value of 16 s. Later, Roetzel et al. [14] found the value of phase lag time as 1.77 s with processed meat.

In order to develop a better tool for predicting the transient temperature profile in tissue, Antaki [15] considered the dual-phase lag (DPL) model to estimate numerically the thermal characteristics time using experimental data in [13]. Subsequently, Liu and Chen [16,17] investigated the existence of DPL thermal behaviour in bio-issue during magnetic hyperthermia. Recently, Liu [18] theoretically studied the temperature rise behaviour in bio-tissue using non-linear form of DPL model during magnetic hyperthermia treatment. Jang et al. [19] demonstrated that the fractional thermal wave model of the bio-heat transfer can provide a unified approach to examine the heat transfer in biological tissue. Liu et al. [20] focussed on the DPL model to analyse thermal response for estimating thermal damage in laser-irradiated biological tissue. They assumed that the transport behaviour of laser light in the tissue is highly absorbed and strongly scattered. Sumit et al. [21] developed DPL-based heat conduction model to investigate the thermal response of laser-irradiated biological tissue phantoms. They also used the LBM-based solution of the coupled RTE and DPL-based numerical model to predict temperature history within the body of the laser-irradiated biological tissue phantoms [22]. Phadnis et al. [23] numerically investigate the thermal response of gold nanoshells-embedded biological tissue phantoms with potential applications into photothermal therapy to destroy the cancerous cells with minimum damage to the surrounding healthy cells. Thus, from the survey literature, it is evident that there have hitherto been no reports of experimentally validated numerical studies that use the DPL model to understand subsurface thermal behaviour in tissue mimics under laser irradiation.

To date, application of gold nanostructures in nanomedicine has extensively been studied. Plasmonicphotothermal therapy that is a minimally invasive oncological treatment, converts photon energy to thermal energy inside nanostructure incubated bio-tissues. Recently, gold nanostructures like gold nanorods, nanospheres as well as carbon nanotubes have been found to enhance the localised photothermal effects by continuous NIR radiation [24–34]. Huang et al. [35] analysed the potential of the enhanced non-linear properties of gold nanospheres for photothermal cancer therapy during short-pulse NIR irradiation. The use of gold mesoflowers for obtaining internal temperature distribution inside bio-tissue, and its effect on collagen ultrastructure by NIR radiation has rarely been investigated. In the present study, two types of nanostructures i.e. gold mesoflowers and nanospheres were used for localised hyperthermia treatment.

This study emphasises the importance of investigating the internal temperature distribution inside tissue mimics embedded with and without gold nanostructures. This work also numerically validates experimental results with DPL model of Pennes bio-heat conduction that takes into account two-phase lags i.e. phase lag time for temperature gradient and heat flux, respectively. Jaunich et al. [36] reported the subsurface temperature enhancement in tissue due to a focussed laser beam. The present study uses a collimated laser beam with beam divergence at 1064 nm less than 4.5 mrad. The topological assessment of bio-tissue (i.e. type I collagen from bovine) at different depths with the corresponding temperature measured has been investigated with atomic force and high-resolution scanning electron microscopy. Next, the functional changes in secondary structures of bio-tissue under NIR radiation have been tracked by Fourier transform infra-red (FT-IR) spectroscopy.

Materials and methods

Materials

Type I collagen extracted and purified for further use from bovine tendon wet tissue (250 mg of pure collagen embedded in 1 g of wet tissue) was procured from Central Leather Research Laboratory, Chennai, India. Aniline (procured from Sigma Aldrich, Mumbai, India) was double distilled before using for chemical process. Ascorbic acid, silver nitrate, cetyltrimethyl ammonium bromide (CTAB), tetrachloroauric acid trihydrate and citric acid were procured from CDH, India, and used as obtained. Double-deionised (DI) water was used throughout the experiments. A continuous wave diode-pumped solid-state laser (MONOPOWER^{TM}) of wavelength 1064 nm was used for experiments.

Experimental methods

To study the effects of topological transformation in collagen microstructures under NIR laser irradiation, an *in vitro* study was conducted employing tissue phantoms. The experimental setup consists of a test acrylic basin which was filled with agar gel to support a glass substrate (illustrated in Figure 1(a) and (b)). The glass substrate was insulated at the bottom surface to prevent the laser beam from passing through and hence the transmitted component of the beam may be considered negligible. It has been further assumed that the laser beam focussed on the hemispherical wet tissue droplet does not encounter any loss across its thickness. To measure the internal temperature distribution in bio-tissue along depth, K type thermocouples were inserted helically along the circumference so that there is no physical contact between them. The thermocouples were placed 2.5 mm distance apart along the depth and the tip of each thermocouple coincided with

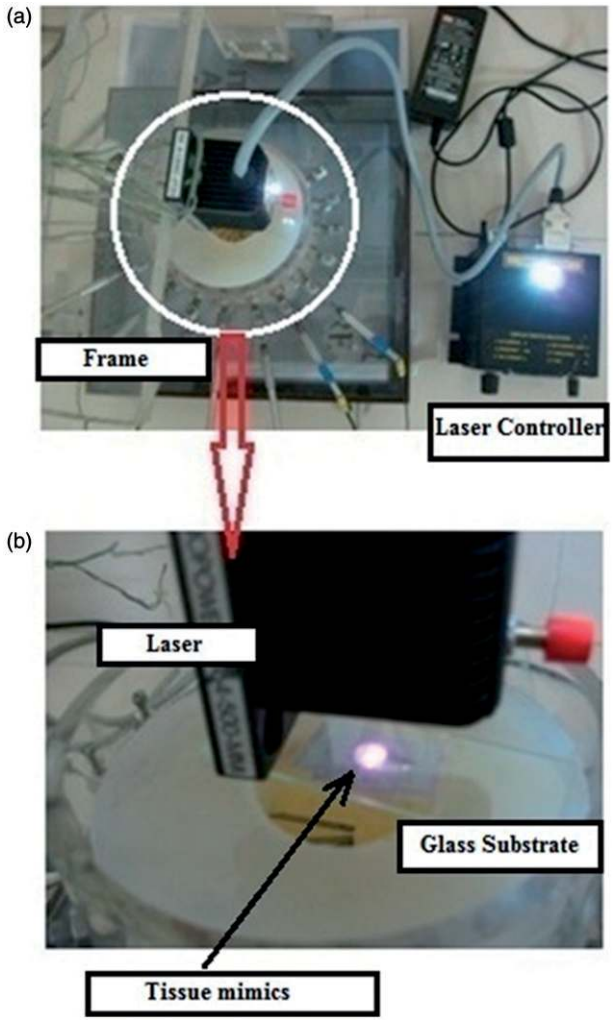

Figure 1. (a) The experimental setup. (b) The encircled mark represents enlarged part of direct heating of collagen gel on glass substrate. The glass slide employed is 75 mm in length and may be used for scale of the figure.

the laser beam's line of propagation. The complete description of experimental setup has been explained in the Supplementary data (Experimental methods) as well as in a previous report by the present authors [37]. The synthesis of gold nanostructures (mesoflowers and nanospheres) was conducted according to the protocol described in published reports by the present authors [38,39]. The absorption spectrum and scanning electron microscopy (SEM) images of the gold nanostructures in question have also been reported in a previous report by present authors [40]. The collagen infused wet tissue was dissolved in 10 mg/ml in 0.05 M acetic acid to obtain collagen in its native acylated state. One drop (a diameter of ~5 mm approx.) of the collagen infused wet tissue embedded with and without gold nanostructures was kept on the glass substrate for laser irradiation to investigate the effects of thermal ablation as well as the effects of concentration of gold nanostructures on the morphology of collagen structure.

Material characterisation

All collagen samples were imaged in the non-contact mode of atomic force microscopy (AFM) at ambient condition. The point probe plus non-contact high resonance (PPP-NCHR) cantilever probe with a radius of curvature< 10 nm and a force constant of 40 N/m was employed for imaging. The silicon probe was procured from Fore-vision Instrument (I) Pvt Ltd, Hyderabad, India. After conducting the thermal irradiation experiments with collagen gel using NIR laser, a 20 μL droplet of the post-irradiated collagen gel was smeared on a cleaned glass substrate and was used for imaging on an XE-100 AFM (Park Systems) system (Hitachi, Tokyo, Japan). A scanner of 5 μm*5 μm with a typical scan rate of 1 Hz was used to produce 256 × 256 pixel images. Apart from using AFM for morphological study of the bio-issue, high-resolution scanning electron microscopy (FEI Quanta FEG 200 HRSEM, Sophisticated Analytical Instrument Facility (SAIF), IIT Madras) was used to image the pre- and post-irradiated collagen fibrils. The FT-IR spectra of native and denaturated collagen embedded with gold mesoflowers were obtained employing a FT-IR spectrometer (Perkin Elmer Instrument Spectrum, Sophisticated Analytical Instrument Facility (SAIF), IIT Madras, Chennai, India). The spectra were recorded in absorption mode at a resolution of 4 cm^{-1} and in the wavelength range of 4000–450 cm^{-1}. For this study, 50 mg of native and denaturated collagen gel were taken to find the functional groups in collagen before and after NIR laser irradiation and their corresponding chemical characteristics. Similarly, 1 mg of gold mesoflowers was homogeneously mixed with 100 mg of KBr for measuring the spectra for the nanostructures in order to isolate the signal from then spectra of mesoflower impregnated collagen.

Mathematical formulation

For the computational study of laser assisted hyperthermia treatment (photothermal therapy), the tumour tissue is considered as a rectangular volume with dimensions of 20 × 20 × 30 mm (illustrated in Figure 2). The tumour tissue is homogeneously impregnated with different gold nanostructures (mesoflowers and nanospheres) where the nanostructure laden tissue properties are considered tuneable parameters within the computational system, based on the type and the concentration. In the present context, the linearised form of DPL model of bio-heat conduction has been implemented to capture the non-Fourier thermal behaviour of bio-tissues. The general Pennes bio-heat transfer equation [7] based on classical Fourier heat conduction in living tissue is expressible as

$$\rho c_p \frac{\partial T}{\partial t} = -\nabla q + \omega_b \rho_b c_b (T_b - T) + Q_{met} + Q_{ext} \quad (1)$$

The equation incorporates the effects of blood circulation and local metabolism on the heat transfer between the internal tissue and the external environment due to the presence of a thermal source. The DPL model of bio-heat conduction considering two effects of thermal inertia and microstructural interaction can be formulated in Cartesian coordinate system as

$$q(x, y, z, t + \tau_q) = -k\nabla T(x, y, z, t + \tau_T) \quad (2)$$

Taking the divergence of Equation (2) and then using $\nabla.q$ in Equation (1), the linearised form of DPL model for tissues

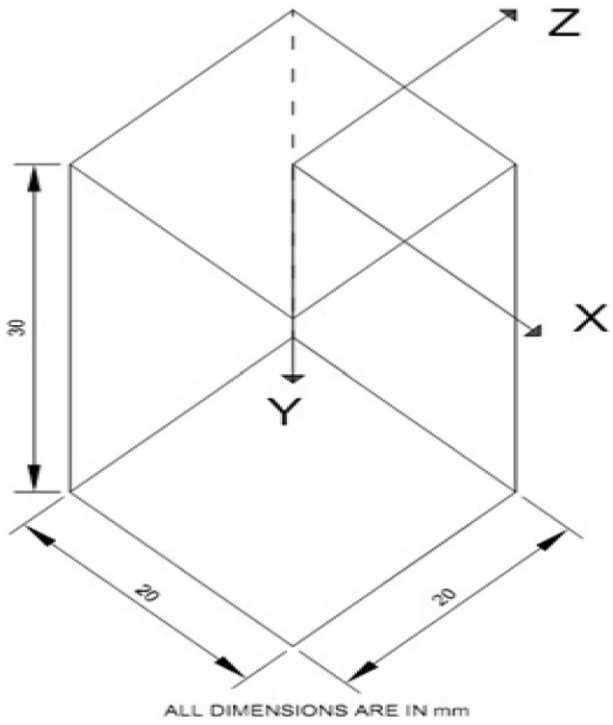

Figure 2. 3D model to predict internal temperature distribution in tissue mimic.

can be expressed as

$$\tau_q \rho c_t \frac{\partial^2 T}{\partial t^2} + (\tau_q \omega_b \rho_b c_b + \rho c_t)\frac{\partial T}{\partial t} = k\nabla^2 T + \tau_T k \nabla^2 \frac{\partial T}{\partial t} + \omega_b c_b \rho_b (T_b - T) + Q_{ext} + Q_{met} + \tau_q \frac{\partial Q_{met}}{\partial t} + \tau_q \frac{\partial Q_{ext}}{\partial t} \quad (3)$$

where ρ is tissue mass density, c_p the specific heat of tissue, Q_{met} the metabolic heat generation, ω_b the blood perfusion rate, c_b the specific heat of blood, ρ_b the mass density of blood and T_b the blood temperature. The spatial heat source is defined as $Q_{ext} = Q_{laser}\ F\ (t)$, where $F(t)$ is a unit step function. The explanation for Q_{laser} has been described in previous report by present authors [37]. The phase-lag times τ_q and τ_T indicate the phase lag of heat flux and temperature gradient, respectively, within the tissue.

The transient bio-heat transfer equation (Equation (3)) was solved for the 3D model of tumour tissue as illustrated in Figure 2. The detailed explanation for grid independence study has been presented in a previous report by the present author. The finer mesh with mesh quality of $q = 0.3601$ is considered for the present computational studies. The boundary conditions provided are as follows: (i) all boundaries except the laser incidence surface are considered to be in Dirichlet condition, (ii) convective heat exchange (heat transfer coefficient h_c=5–25 W/m^2 K) [41] with surrounding ambient air by natural convection was considered at the top surface, (iii) blood perfusion and thermal evaporation and/or phase change of present tissue phantom model during heat transfer process were considered to be negligible, (iv) the tissue's optical and thermal properties obtained from [4] were considered to be constant during the heat transfer process, and (v) the optical parameters α and β were obtained from [29]. The computations were carried out using COMSOL Multiphysics software [42] with conjugate linear system solver and algebraic multi-grid pre-conditioner. The temperature tolerance was kept at the value of 0.0001 °C throughout the simulations with time step of 0.01 s.

Table 1. Thermo-physical properties of tissue phantom [4].

Density (ρ)	Thermal conductivity (k)	Specific heat (c_t)
1050 kg/m^3	k = 0.5 W/m K	3700 J/kg K

Table 2. Optical properties of tissue phantom [40].

Optical properties	Scattering coefficient (β)	Absorption coefficient (α)
Bare tissue	$\beta = 530$ m^{-1}	$\alpha = 50$ m^{-1}
Tissue embedded with nanoparticles	$\beta = 530$ m^{-1}	$\alpha = 300$ m^{-1}

In the following simulations, the laser intensities at the tissue surface (at the origin of 3D model as shown in Figure 2) I_o are considered as 3.5×10^4 W/m^2 (corresponding to laser power 446 mW) and 4.4×10^4 W/m^2 (corresponding to laser power 558 mW), respectively. The beam radius at (0, 0) i.e. at the origin was 2 mm. The thermo-physical and optical properties of tissue phantom are given in Tables 1 and 2, respectively.

Results

Non-Fourier effect in bio-tissues

As a consequence of comprehending the non-homogeneous inner structure property of bio-tissues (i.e. type I collagen in present experiments), several researchers in the field have claimed that propagation speed of thermal signals in bio-tissue is finite, which in turn indicates non-Fourier behaviour which is characterised via the thermal relaxation time. Consequently, it must differentiate the temperature gradient developed inside tissue as predicted by classical Fourier and DPL model of heat conduction. For simulating the thermal response within a rectangular tumour tissue, the present work considers the linearised form of DPL model with phase lag (i.e. τ_q and τ_T) values as 16 s and 0.045 s [13]. The temperature variation with depth without the presence of gold nanostructures for laser power of 446 mW and 558 mW have been illustrated in Figures 3 and 4, respectively. It is observed that the temperature increases up to certain depth from the surface and then decreases gradually. Such an unusual phenomenon of temperature rise is observed to be well predicted by DPL model of Pennes bio-heat model compared with the classical Fourier model, considering the source term model by the present authors [37].

The numerical results predicted by classical Fourier model deviate quantitatively with experimental results compared with the DPL model. It is observed that the region of temperature rise along depth is accurately predicted by the DPL model, whereas the decrease in temperature is predicted well by the Fourier conduction based Pennes bio-heat model. This shows that the forward scattering phenomenon

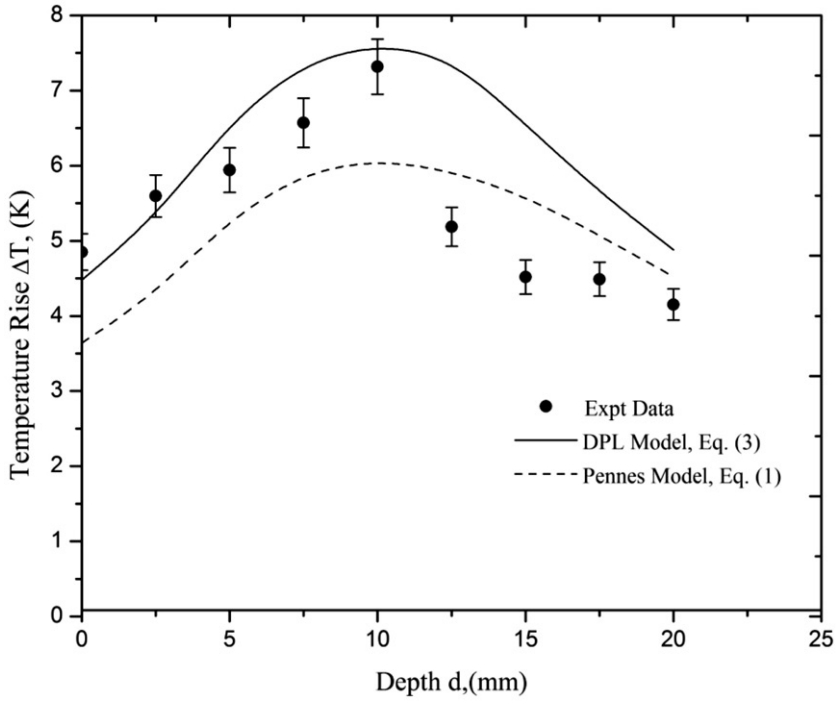

Figure 3. Temperature distribution in collagen gel with an incident power of 446mW after 400 s.

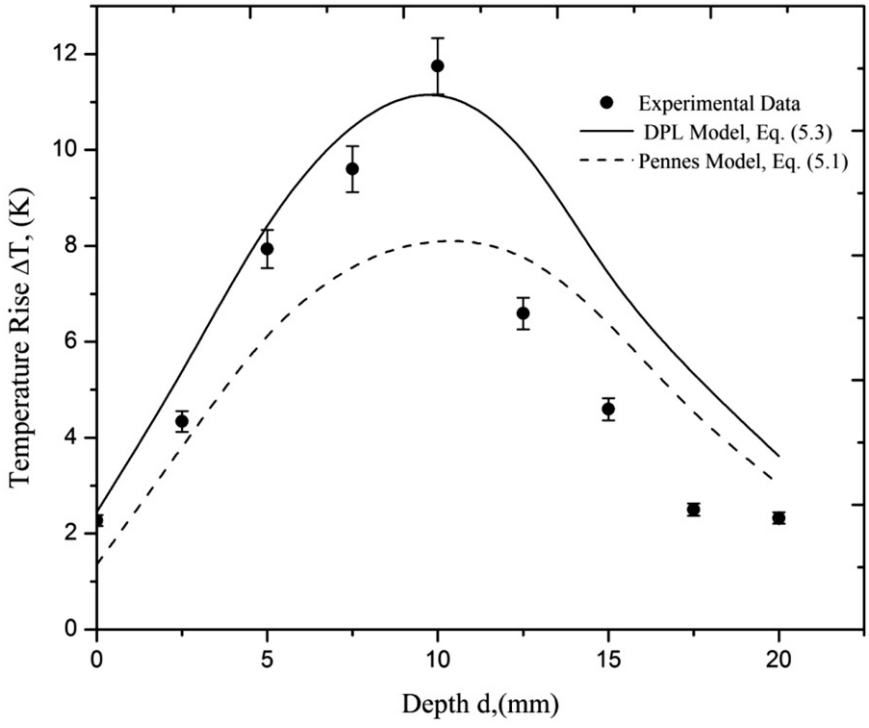

Figure 4. Temperature distribution in collagen gel with an incident power of 558 mW after 400 s.

occurring inside tissue medium [37] does not follow hyperbolic conduction effect once the thermal peak is achieved. However, the backscattering behaviour is depicted well by the non-Fourier effect and, therefore, is the component of irradiation which induces the non-Fourier effects during propagation. The spatial heating source developed by the authors in their earlier work considers the multiple scattering phenomena in bio-tissues. Collimated laser beam focuses on the surface of the tissue phantom. It specifically undergoes coherent backscattering by restricting spread in the beam path, causing enhanced absorption inside the tissue. The external source term contains three terms i.e. the Gaussian profile of the laser beam, the attenuation of beam due to absorption, and the re-enhancement of photon density at a distance along depth. The last two terms compete to result in the peak photon intensity at a particular depth which is a function of absorption coefficient and scattering coefficient. The back scattering is dominant over the forward scattering

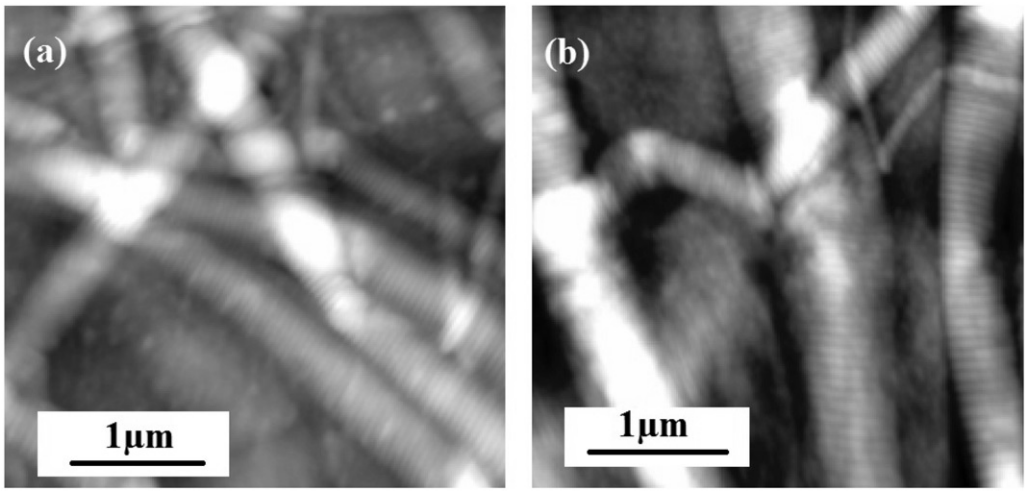

Figure 5. Atomic force microscopy (AFM) topography images of (a) native collagen and (b) collagen microstructure after laser irradiation with an incident power of 446 mW and laser exposure time of 400 s.

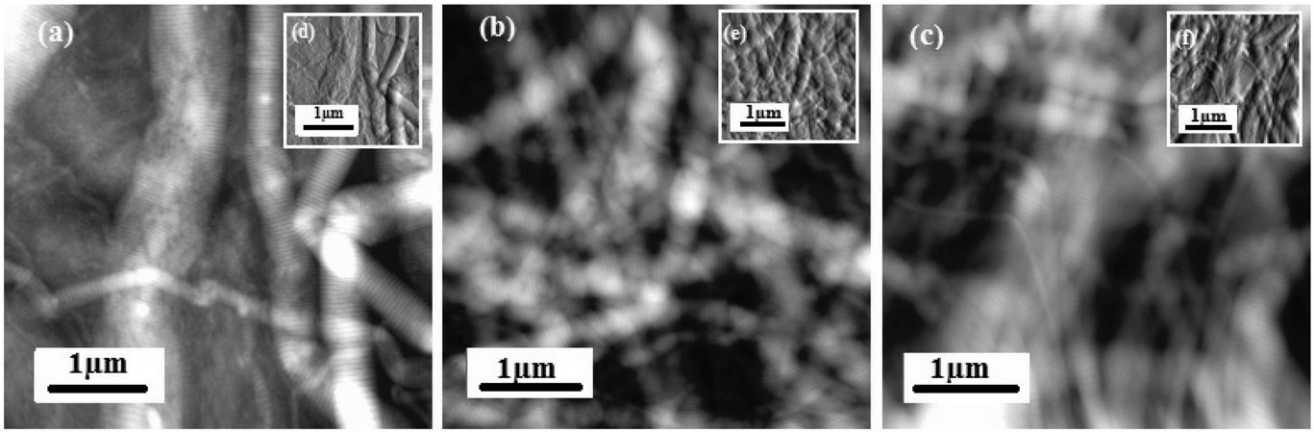

Figure 6. Atomic force microscopy topography images of (a) at surface and (b) depth of maximum temperature. (c) Depth beyond the maximum temperature without embedded gold nanostructures after 400 s and with an incident power of 446 mW. (d), (e), and (f) Inset: AFM error signal image without embedded gold nanostructures after 400 s and with an incident power of 446 mW.

while the photon travels deeper inside the tissue phantom. Second, the extra term $\tau_T k \nabla^2 \frac{\partial T}{\partial t}$ involved in the linearised form of DPL model for tissues (Equation (3)) enhances the temperature rise during early time of heating as reported in the literature. Therefore, the hyperbolic model does not predict well the decreasing profile of temperature distribution after the peak because the weakened beam intensity leads to reduced scattering, causing the Fourier model to provide quite good predictions below the peak depth. However, such initial increase in temperature validated with hyperbolic conduction behaviour is observed for the first time to the best of the authors' knowledge as supported by detailed literature survey. The damage to the collagen ultrastructure was qualitatively assessed with AFM and Figures 5 and 6, respectively, show damage to collagen microstructures subjected to different incident laser power (i.e. 446 mW and 558 mW). It is observed that the damage to bio-tissue at depth of maximum temperature is qualitatively higher in comparison with that at the surface and at a depth higher than that with maximum temperature at incident power of 558 mW compared with incident power of 446 mW. This further concretised the thermal readings obtained during experiments. The apparent ablation of collagen fibrillar microstructure under laser irradiation is obvious in case of 558 mW, which puts forward the importance of laser power and accurate heat transfer model in living tissues for accurate hyperthermia treatment to achieve proper necrosis.

Potential of gold naonostructures on collagen microstructure by NIR laser irradiation

The next objective is to investigate the effect of concentration of gold mesoflowers on tissue mimics with laser irradiation. Irradiation is performed with incident power of 502 mW and embedded with two concentrations of gold mesoflowers (2 g/kg and 3 g/kg of wet tissue).The HRSEM image of collagen microstructure in Figure 7(c) shows the presence of cross-linking in collagen ultrastructures after irradiation without embedded gold mesoflowers, i.e. the micro-fibrils only undergo dehydration process which is considered as the first stage of denaturated collagen (Figure 8(a) and (b), respectively). In case of different concentrations of mesoflowers embedded within tissue, it is observed that the separation of two micro-fibrils occurs (Figure 7(b)) upon laser

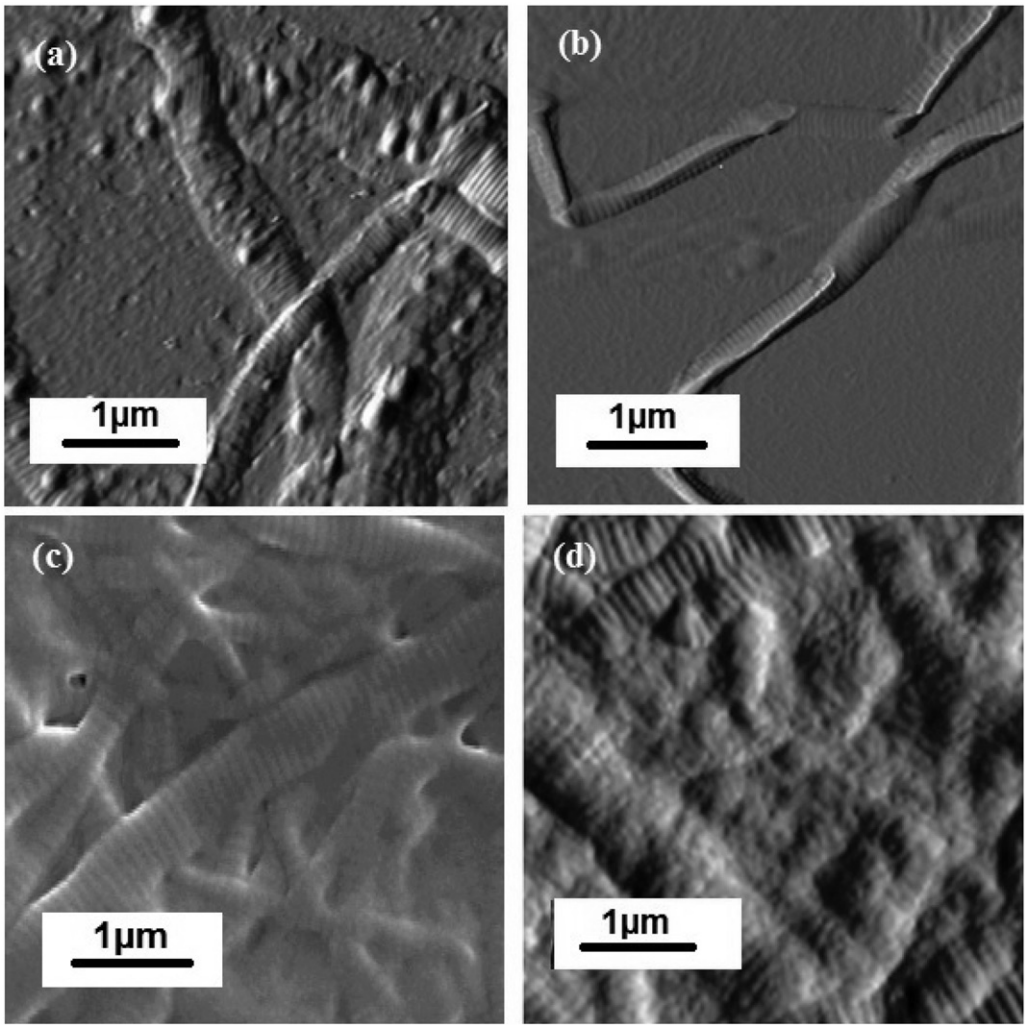

Figure 7. Atomic force microscopy error signal images (a) native collagen embedded with mesoflowers (i.e. 2 g/1 kg of wet tissue) without heating and (b) denaturated collagen at the same concentration with an incident power of 502 mW. (c) High-resolution scanning electron microscopy image of denaturated collagen without nanostructures with an incident of 502 mW and (d) denaturated collagen with concentration of 3 g/1 kg of wet tissue with same incident power. In all cases, the laser exposure time is 400 s.

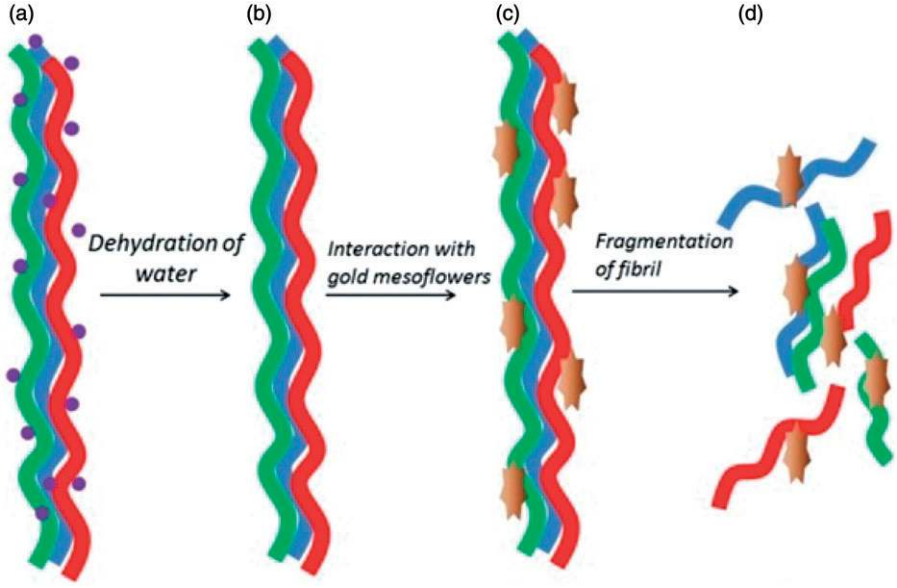

Figure 8. Illustration of (a) hydrated collagen containing hydrogen bonds, (b) dehydrated state of collagen due to breakage of interchain water bonds effected by NIR laser irradiation, (c) native collagen embedded with gold mesoflowers, and (d) severe loss of intrachain bonded water and fragmentation of constituent peptides by NIR radiation.

irradiation which is possibly because the thermal energy generated within the phantom leads to thermal straining the fibrils along the length, leading to structural disruption. Second, with higher concentration of mesoflowers, the fragmentation of collagen microstructures occurs, since the biological system is exposed to electromagnetic radiation (due to the plasmonic interactions of gold nanostructures with the incident photons), due to which generation of free radicals by electron transfer reactions [43] occurs at the side chains. The formation of super-oxide anion (O_2^-), non-radical hydrogen peroxide (H_2O_2), and non-selective strong oxidisers like hydroxyl radicals [44] cause different reactions such as hydrogen abstraction and fragmentation in the collagen microstructure (Figures 7(d) and 8(c) and (d), respectively). The collagen microstructures also undergo cross-link breakage due to non-enzymatic glycosylation of lysine and hydroxylysine residues and disulphide bridges [45]. This is also plausible due to disruption of water bridges at the intermolecular and intramolecular level during enhanced thermal transport caused by the nanostructures. The existence of water bridges, which increases the thermal stability, has been experimentally reported for the collagen model peptide [46] and is the possible reason why cross-link breakage is observed only in case of plasmonic hyperthermia where higher thermal transport occurs.

It, therefore, becomes necessary to investigate the effects of gold nanostructures (i.e. mesoflowers and nanospheres) on the internal temperature distribution within tissue mimics under laser irradiation for plasmonic photothermal therapy. Figure 9 shows the temperature distribution in bio-tissue in presence of gold mesoflowers and compared with the modelling results that considered non-Fourier conduction model with phase-lag values of $\tau_q = 16$ s and $\tau_T = 0.045$ s [13]. The phenomenon observed without nanostructures as explained in the earlier paragraph is similar in the present case, but enhancement in temperature rise in tissue mimics is more due to the presence of gold mesoflowers for the same incident power of 446 mW. This study investigates about the effect of temperature rise on tissues in presence of nanostructures at macro and molecular level. Damage to collagen ultrastructure corresponding to respective depth wise temperature was quite extensive for concentration of 2 g/1 kg of wet tissues in Figure 10, compared with the results observed without mesoflowers and with powers of 446 and a laser exposure time of 400 s. This suggests that the effect of mesoflowers for localised hyperthermia treatment for a lower power is vital compared with high incident power which may cause more damage to nearby healthy tissues. Similar observation of temperature rise in tissues was also found with the concentration of gold mesoflowers and nanospheres (i.e. 3 mg/1 kg of wet tissue) for an incident power of 446 mW as shown in Figures S2 and S3 in Supplementary data, respectively.

Observation of axial D-periodicity under NIR laser irradiation

Next the effect of NIR radiation on the axial D-periodicity of collagen fibril was investigated. Figure 11 shows the images of denaturated collagen embedded with and without gold mesoflowers and variable incident power after 400 s. While observing the image shown in Figure 11(C) compared with Figure 11(A) and (B), respectively, the denaturation to bio-tissues due to the presence of gold nanostructures is seen to be severely pronounced. As reported earlier [47], the axial

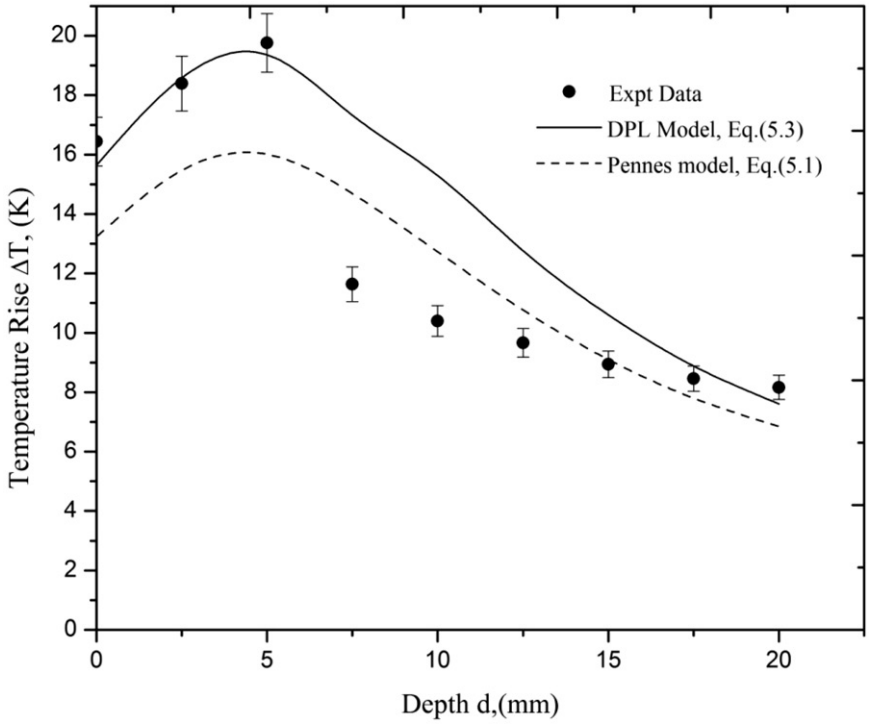

Figure 9. Temperature distribution in collagen gel embedded with 2 g/1 kg of wet tissue concentration of gold mesoflowers, and with an incident power of 446 mw after 400 s.

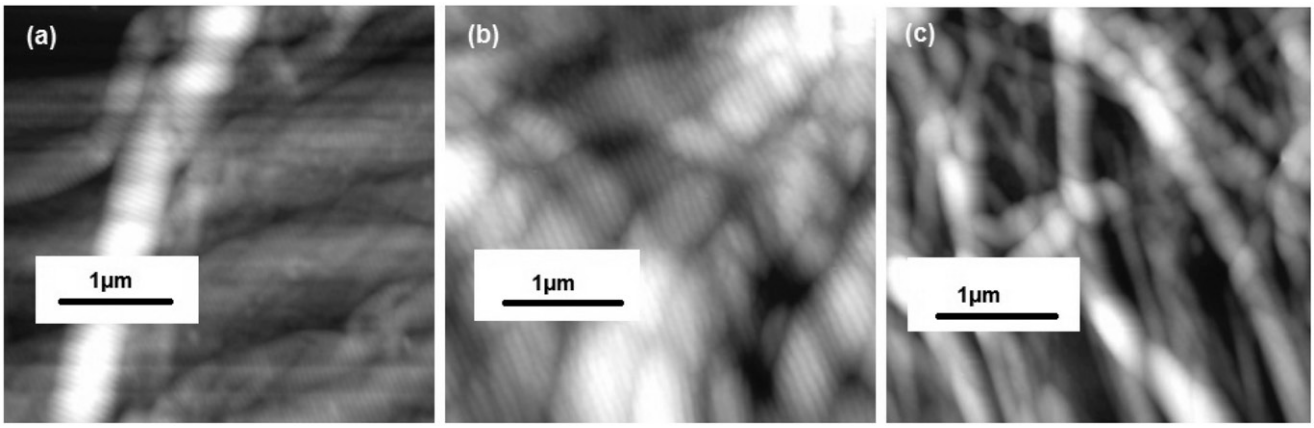

Figure 10. Atomic force microscopy topography images of (a) at surface, (b) depth of maximum temperature, and (c) depth beyond the maximum temperature with concentration of 2 g/1 kg of wet tissue after 400 s and with an incident power of 446 mW.

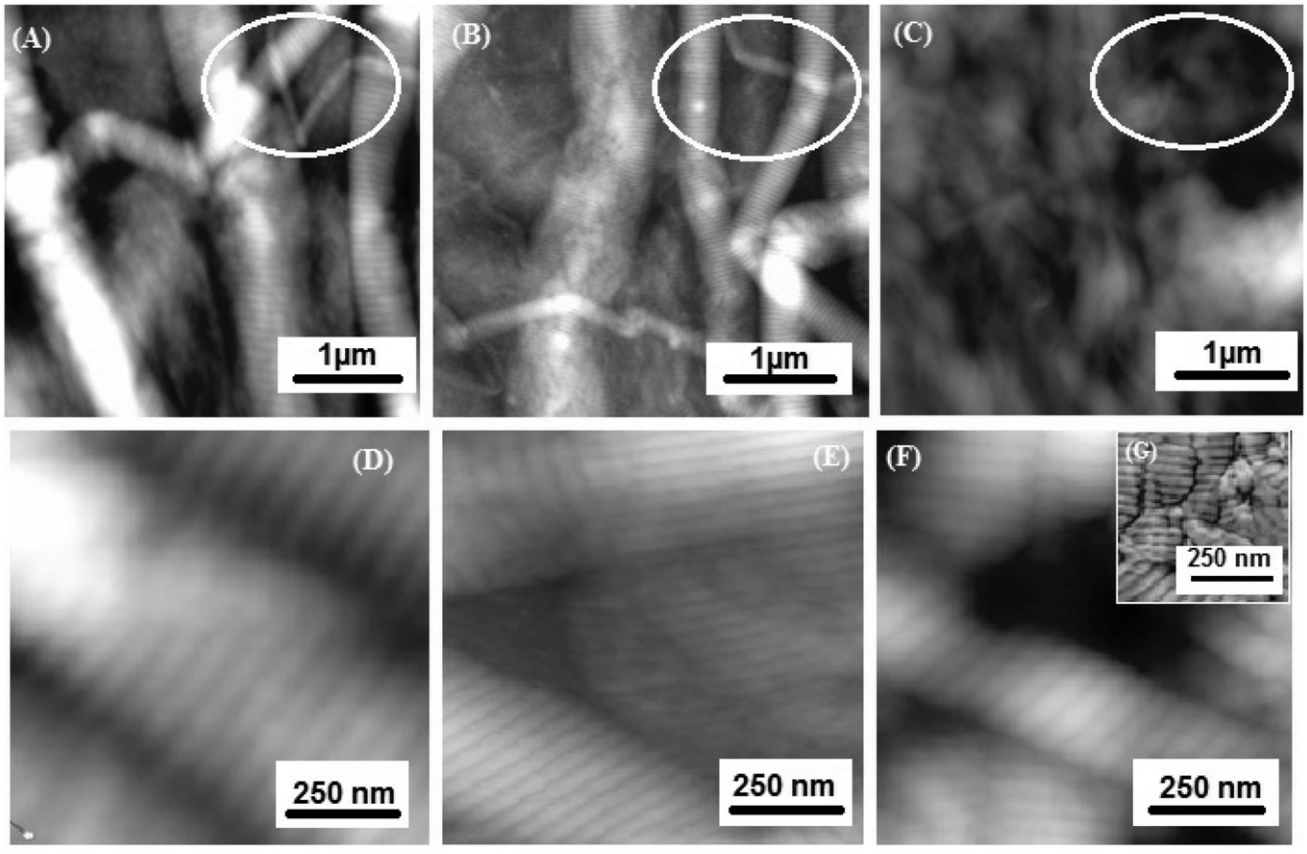

Figure 11. Atomic force microscopy (AFM) topography images of (A) at surface with incident power of 446 mW, (B) at surface with an incident power of 558 mW without embedded with gold mesoflowers, and (C) at surface with an incident power of 446 mW and a concentration of 3 g mesoflowers/1 kg of wet tissue after 400 s and with an incident power of 446 Mw. Similarly, (D), (E), and (F) show the encircled portion at 250 nm scale bar. (G) Inset: AFM error signal image at surface with an incident power of 446 mW and a concentration of 3 g mesoflowers/1 kg of wet tissue after 400 s and with an incident power of 446 Mw.

D-periodicity of fibril decreases as the triple helix ultrastructure undergoes unfolding at the gap zone of collagen fibril as this region is thermally less stable. Since gold mesoflowers are present on the surface of micro-fibril (see Figure 7(a)), the thermal energy generated due to laser interaction affects the gap zone strongly as it consists of the cooperative unit (i.e. a domain which is free of stabilising hydroxyproline residues). Under thermal radiation, all the α-chain hydrogen bonds are broken in this unit and the separate chains are free to mutilate in this gap zone [48]. The random fragmentation of micro-fibrils is clearly observed in Figure 11(G) (i.e. inset figure), where with 3 g of mesoflowers/1 kg of wet tissue, the breakage of water bridges involved in the aggregation of collagen molecules as well as water molecules for stabilisation and formation of triple helix structure as explained in [49] is evident. The present study shows that the reduction in periodicity as measured is obtained as $D = 45.053 \pm 5.187$ (see Table 3) during transient heating process for 400 s and with an incident power of 446 mW, while its value in native state is $D = 66 \pm 2.3$nm (the number

of samples observed =64). Few earlier studies also predict similar observation on rat-tail collagen during constant temperature heating process [47,50]. Conclusively, the axial periodicity of collagen is independent of medium of heating but depends on hydration of fibril and, therefore, is a direct biophysical consequence of thermal ablation during hyperthermia.

Molecular structure of denaturated collagen ultrastructures

In previous report by present authors, the importance of increased subsurface temperature towards photothermal therapy [40] was suggested. However, that study did not delineate the non-Fourier thermal effect to collagen structural hierarchy and change in vibration characteristics of chemical functional groups subjected to electromagnetic radiation. To analyse the secondary structure of native and denaturated collagen corresponding to collagen at respective depths (i.e. at surface, depth of maximum temperature and depth below that with maximum temperature) and the different bands related to peptide linkages of collagen are reported in the present work. Since the temperature rise at depth of maximum temperature is much steep compared with surface temperature rise with an incident power of 446mW and mesoflower concentration of 3 g/1 kg of wet tissues (see Figures S4 in Supplementary data), it is equally important to analyse the secondary structures. In the subsequent section, FT-IR spectral characteristics of different bands are explained in details and the direct biophysico-chemical aspects of hyperthermia therapy on the tissue structure has been put forward.

Table 3. Property values of native and denaturated collagen.

State of tissue mimics	Present experimental results axial periodicity (D) in nm	Bozec et al. [43] results axial periodicity (D) in nm	Reference
Native collagen	66 ± 2.3	67.8 ± 2.4	[47]
Denaturated collagen	45.053 ± 5.187	38 ± 10	[47]

Observation of amide A band components

The FT-IR spectral characteristics of bands are shown in Figures 12 and 13. The amide A band of collagen is usually observed at 3330–3325 cm^{-1} and is associated with NH-stretching and OH groups [51–54]. In the present FTIR study, the band of amide A is absent in native collagen (see Table S4 in Supplementary data). Kaminska et al. [55] reported that the frequency of amide band generally decreases as protein structural order decreases. The changes in band of denaturated collagen after being exposed to laser irradiation at different depth are shown in Table S5 (Supplementary data), which agrees well with the above statement. Present results suggest that there is larger shift in band at depth of maximum temperature compared with the band values at surface and depth beyond maximum temperature. After exposure to NIR irradiation, the band 3330 cm^{-1} of the native state decreases to 3323, 3321, 3312, and 3305 cm^{-1} at different depths. This in turn shows the extensive damage to tissue mimic from surface to interior region of tissue, associated with either scission of backbone amide bonds or the side chain amides. The above observation is consistent with the fact that 254 nm UV is capable of breaking C–N bonds and

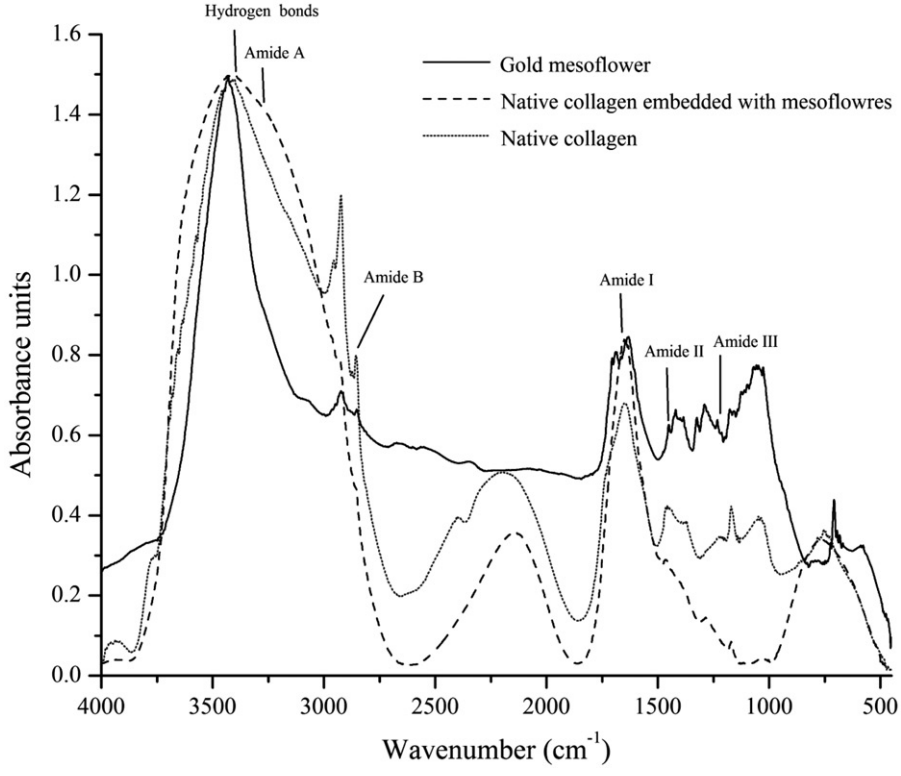

Figure 12. Fourier transform infrared (FTIR) spectral study of collagen (native collagen versus collagen embedded with gold nanostructures).

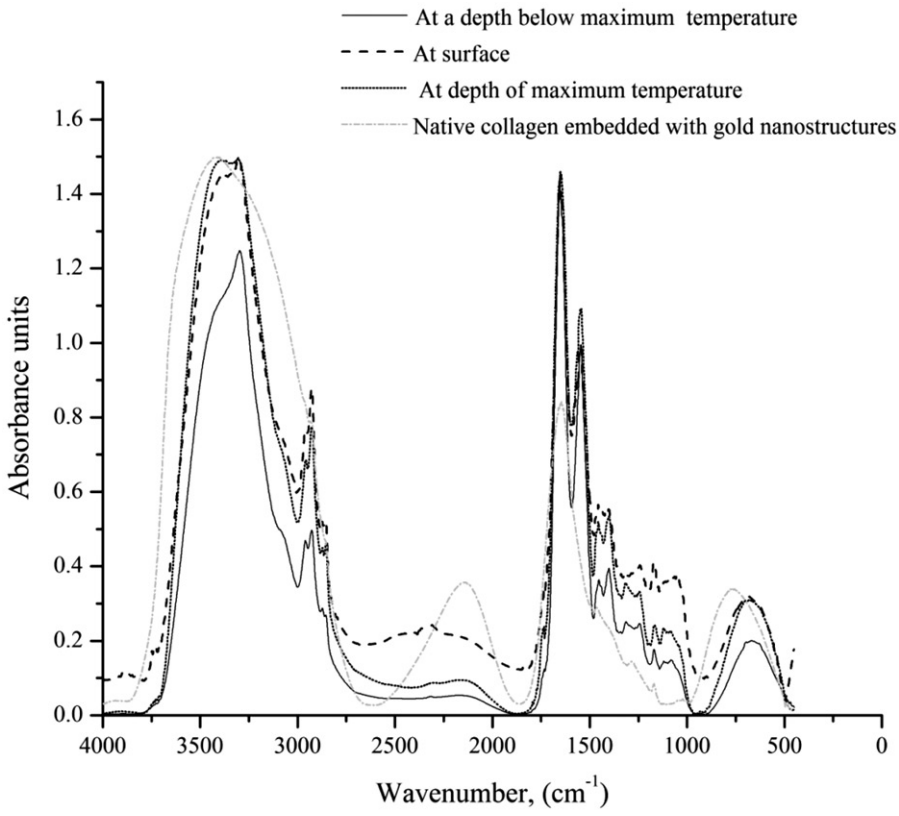

Figure 13. FTIR spectral study of denaturated collagen under NIR laser irradiation.

causing the scission of peptide bonds [56]. The bands at 2946 cm^{-1} and 2875 cm^{-1} observed in native collagen are assigned to the CH_3-asymmetric vibration mode and CH_2-asymmetric vibration mode, respectively. After NIR treatment, the position of the band shifted to a lower frequency indicating the alternation of bonds or breakage of side chains of amino acid. As reported in [53], the band at 3080 cm^{-1} usually denotes the amide B band of native collagen. Even though this band is absent in the present experiment, after laser irradiation, the band position shifted largely to 2960 cm^{-1} and 2959 cm^{-1} at the respective depth. This represents the scission of N–H bonds, whereas this observation is not found after UV treatment in [57], which signifies that thermal ablation is more potent in structural scission, leading to necrosis.

Observations of amide I band components

The amide I band resulting from the stretching vibration of the peptide carbonyl group (–C = O) along with the polypeptide backbone shows three peaks at 1648 cm^{-1}, 1650 cm^{-1}, and 1660 cm^{-1} in native collagen embedded with and without gold nanostructures (see Table S4 in Supporting information). The most intensive band observed at 1660 cm^{-1} indicates the collagen native triple helix [51,58], whereas after laser irradiation, the amide I peak possesses an intense band at 1643 cm^{-1}. In this case, the decreasing values of absorbance along tissue depth lead to breaking of backbone and amide carbonyls. The FTIR study shows the amide II band peaks at 1547 cm^{-1}, 1549 cm^{-1}, and 1560 cm^{-1} representing the amide groups of triple helical state [56–58]. It is interesting to observe that the shifting of amide II band compared with native state after NIR laser irradiation is 1 cm^{-1} at the depth of maximum temperature, but at surface and depth beyond maximum temperature, this band indicated no changes after exposure to NIR laser irradiation. Hydrogen abstraction or structural scission is proposed to be at the crux of this observed phenomenon. Similarly, the amide III band was shifted from 1243 cm^{-1} to 1217 cm^{-1} and 1247 cm^{-1}, respectively, for the present FTIR study. Hence, the above discussions regarding the degradation of native collagen upon NIR radiation imply how accurate measurement and prediction of temperature is important for localised photothermal therapy from the point of view of thermophysical damage to the carcinoma.

Effect of different source models on internal temperature distribution

Figure 14 compares computational studies of Welch's attenuating photon intensity profile model and the present multiple scattering model as source terms considering DPL model of Pennesbio-heat equation with relaxation times τ_q=16 s and τ_T= 0.045 s [13], respectively. This clearly illustrates that the present source term based on multiple scattering theory compared with Welch model of light propagation in tissue is in good agreement with experimental results. Hence the computational study suggests that the theoretical model developed to explain the spatial distribution of temperature can also be immensely helpful for photothermal therapy by predicting the optimal temperature and damage in tumour as well as in healthy tissues in addition to understanding then biophysical changes at the microscopic level.

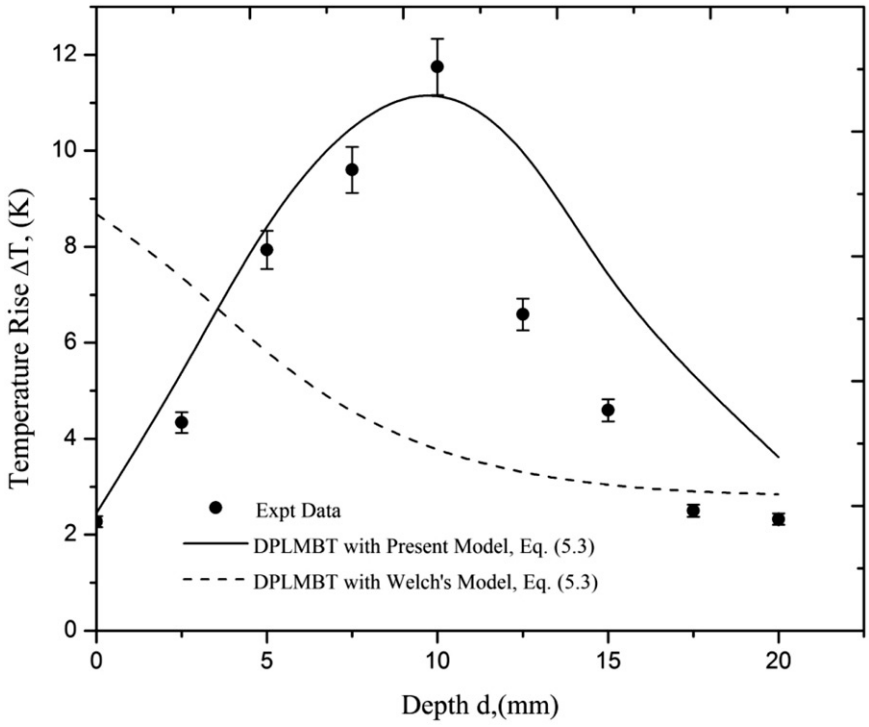

Figure 14. Effect of source term for light propagation in tissue under laser irradiation with an incident power of 558 mW and laser exposure time of 400 s.

Conclusions

To infer, the potential of gold nanostructures towards targeted photothermal therapy has been investigated from different aspects with major stress on understanding the biophysical damage at the microscale in tissue phantoms. With varying concentrations of gold nanostructures, the enhancement in temperature rise was computationally modelled with DPL model of bio-heat transfer equation in tissue mimic using NIR electromagnetic radiation. The micro-scale, non-classical heat transfer effects (non-Fourier heat conduction) on bio-tissue mimicking tumour incubated with plasmonic nanostructures is vital for accurate measurement of temperature. It is overall found that the gross deviations in temperature rise between the DPL model and Fourier model of heat conduction at the peak with experiments conducted in pure collagen are 1 °C and 4 °C, respectively, which further proves that non-Fourier effects in the tissue pose equal importance as the requirement for a correct laser heating model. Similarly, the temperature rise between the DPL model and the Fourier model of heat conduction at the peak with experiments conducted in tissue phantoms embedded with nanoparticles are 0.5 °C and 4 °C, respectively. This emphasises to focus on different thermal models to predict accurate temperature distribution in bio-tissues which otherwise may lead to damage of healthy tissue and will be unrealistic from clinical aspects. Under thermal denaturation, the damage to tissue mimics at the respective depth wise temperature measured was experimentally assessed with atomic force and HR scanning electron microscopy. This qualitative study of damage was complemented and augmented by a further FTIR study to find out the secondary structures in the collagen phantom. Experimental temperature distribution, AFM, and FTIR studies suggest the importance of NIR electromagnetic radiation effect on cancerous tissue for targeted photothermal therapy. Severe damage to the collagen structures due to thermal scission as well as dehydration induced by the enhanced thermal transport by the plasmonic nanostructures sheds insight onto the biophysical nature of hyperthermia which is rare in the literature but is of prime importance for clinical approaches. The present study helps cementing the knowledge towards thermal ablation of carcinoma by minimising the damage to the healthy tissue with insight into the microscopic physico-chemical processes during such therapy. The study may also contribute to microstructural aspects of tissue damage and wound repair.

Acknowledgements

The authors thank late Dr. P.K. Sehgal of the Central Leather Research Laboratory, Chennai, India, for providing the collagen and Dr. Shamit Bakshi, Mechanical Engineering Department, IIT Madras for providing the laser. N. S. thanks Dr. T. Pradeep's group, Chemistry Department, IIT Madras for help with the preparation of gold nanostructures.

Disclosure statement

The authors declare no conflict of interest with respect to the present paper.

References

[1] Tuan VD. (2003). Biomedical photonics handbook. Boca Roton, FL: CRC Press.

[2] Diagaradjane P, Shetty A, Wang JC, *et al.* (2008). Modulation of in vivo tumor radiation response via gold nanoshell-mediated vascular-focused hyperthermia: Characterizing an integrated

antihypoxic and localized vascular disrupting targeting strategy. NanoLetters 8:1492–500.
[3] Feng Y, Fuentes D, Hawkins A, *et al*. (2009). Nanoshell-mediated laser surgery simulation for prostate cancer treatment. Engin Comp 25:3–13.
[4] Maltzahn MV, Park J, Agarwal HA, *et al*. (2009). Computationally guided photothermal tumor therapy using long-Circulating gold nanorod antennas. Canc Res 69:3892–900.
[5] Dasgupta D, Maltzahn G, Ghosh VS, *et al*. (2009). Probing nanoantenna-directed photothermal destruction of tumors using noninvasive laser irradiation. Appl Phys Lett 95:233701–6.
[6] Bayazitaglou Y. (2009). Nanoshell assisted cancer thermal therapy: numerical simulations. Proceedings of the ASME 2nd Micro/Nanoscale Heat Mass Transfer International Conference, 18546.
[7] Pennes HH. (1948). Analysis of tissue and arterial blood temperature in the resting Forearm. J Appl Physiol 1:93–122.
[8] Dai T, Pikkula BM, Wang LV, Anvari B. (2004). Comparison of human skin opto-thermal response to near-infrared and visible laser irradiations: a theoretical investigation. Phys Med Biol 49:4861–77.
[9] NickelHermann S, Essenpreis MM, Farrell T, *et al*. (2000). Anisotropy of light propagation in human skin. Phys Med Biol 45:2873–86.
[10] Graßmann A, Peters F. (1999). Experimental investigation of heat conduction in wet sand. Heat Mass Trans 35:289.
[11] Herwig H, Beckert K. (2000). Experimental evidence about the controversy concerning Fourier or non-Fourier heat conduction in materials with a non-homogeneous inner structure. Heat Mass Trans 36:387–92.
[12] Kaminiski W. (1990). Hyperbolic heat conduction equation for material with a nonhomogenous inner structure. ASME J Heat Trans 112:555–60.
[13] Mitraa K, Kumar S, Vedavarz A, Moallemi MK. (1995). Experimental evidence of hyperbolic heat conduction in processed meat. ASME J Heat Trans 112:555–73.
[14] Roetzel W, Putra N, Das SK. (2005). Experiment and analysis for non-Fourier conduction in materials with non-homogeneous inner structure. Int J Thermal Sci 42:541–52.
[15] Antaki PJ. (2005). New interpretation of non-Fourier heat conduction in processed meat. J Heat Trans 127:189–93.
[16] Liu KC, Chen HT. (2010). Investigation for the dual phase lags behaviour of bio-heat transfer. Int J Thermal Sci 49:1138–46.
[17] Liu KC, Chen HT. (2009). Analysis for the dual phase lag bio-heat transfer during magnetic hyperthermia treatment. Int Heat Mass Trans 52:1185–92.
[18] Liu KC. (2011). Nonlinear behavior of thermal lagging in concentric living tissues with Gaussian distribution source. Int J Heat Mass Trans 54:2829–36.
[19] Jiang X, Qi H. (2012). Thermal wave model of bioheat transfer with modified Riemann–Liouville fractional derivative. J Phys A: Math Theor 45:485101.
[20] Liu KC, Wang JC. (2014). Analysis of thermal damage to laser irradiated tissue based on the dual-phase-lag model. Int J Heat Mass Trans 70:621–8.
[21] Kumar S, Srivastava A. (2015). Thermal analysis of laser-irradiated tissue phantoms using dual phase lag model coupled with transient radiative transfer. Int J Heat Mass Trans 90:466–79.
[22] Patidar S, Kumar S, Srivastava A, Singh S. (2016). Dual phase lag model-based thermal analysis of tissue phantoms using lattice Boltzmann method. Int J Thermal Sci 103:41–56.
[23] Phadnis A, Kumar S, Srivastava A. (2016). Numerical investigation of thermal response of laser-irradiated biological tissue phantoms embedded with gold nanoshells. J. Therm Biol 61:16–28.
[24] Kennedy LC, Bickford LR, Lewinski NA, *et al*. (2011). A new era for cancer treatment: gold-nanoparticle-mediated thermal therapies. Small 7:169–83.
[25] Huang X, El-Sayed IH, El-Sayed Method MA. (2010). Applications of gold nanorods for cancer imaging and photothermal therapy. Mol Biol 624:343–57.
[26] Loo CA, Lowery A, Halas N, *et al*. (2005). Immunotargeted nanoshells for integrated cancer imaging and therapy. NanoLetters 5:709–11.
[27] Huang X, El-Sayed IH, Qian W, El-Sayed MA. (2006). Cancer cell imaging and photothermal therapy in the near-infrared region by using gold nanorods. J Am Chem Soc 128:2115–20.
[28] Dickerson EB, Dreaden E, Huang C, *et al.* (2008). Gold nanorod assisted near-infrared plasmonic photothermal therapy (PPTT) of squamous cell carcinoma in mice. Canc Lett 269:57–66.
[29] Huang X, Jain PK, El-Sayed IH, El-Sayed MA. (2008). Plasmonic photothermal therapy (PPTT) using gold nanoparticles. Lasers Med Sci 23:217.
[30] El-Sayed IH, Huang X, El-Sayed MA. (2006). Selective laser photothermal therapy of epithelial carcinoma using anti-EGFR antibody conjugated gold nanoparticles. Cancer Lett 239:129–35.
[31] Xu X, Meade A, Bayazitoglu Y. (2011). Numerical investigation of nanoparticle-assisted laser-induced interstitial thermotherapy toward tumor and cancer treatments. Lasers Med Sci 26:213–22.
[32] Zhou F, Xing D, Ou Z, , *et al*. (2009). Cancer photothermal therapy in the near-infrared region by using single-walled carbon nanotubes. J Biomed Opt 14:021009.
[33] Burkea A, Dingb X, Singha R, *et al*. (2009). Long-term survival following a single treatment of kidney tumors with multiwalled carbon nanotubes and near-infrared. Proc Natl Acad Sci 106:12897.
[34] WongKam N, O'Connell SM, Wisdom JA, Dai H. (2005). Carbon nanotubes as multifunctional biological transporters and near-infrared agents for selective cancer cell destruction. Proc Natl Acad Sci 102:11600.
[35] Huang X, Qian W, El-Sayed H, El-Sayed MA. (2007). The potential use of the enhanced nonlinear properties of gold nanospheres in photothermal cancer therapy. Laser Surg Med 39:747–53.
[36] Jaunich M, Raje S, Kim K, *et al*. (2008). Bio-heat transfer analysis during short pulse laser irradiation of tissues. Int J Heat Mass Trans 51:5511–21.
[37] Sahoo S, Ghosh N, Narasimhan SA, Das SK. (2014). Investigation of non-Fourier effects in bio-tissues during laser assisted photothermal therapy. Int J Therm Sci 76:208–20.
[38] Sajanlal PR, Sreeprasad TS, Nair AS, Pradeep T. (2008). Wires, plates, flowers, needles, and core−shells: diverse nanostructures of gold using polyaniline templates. Langmuir 24:4607–14.
[39] Sajanlal PR, Pradeep T. (2009). Mesoflowers: a new class of highly efficient surface-enhanced Raman active and infrared-absorbing materials. Nano Res 2:306–20.
[40] Ghosh S, Sahoo N, Sajanlal PR, *et al*. (2014). Anomalous subsurface thermal behavior in tissue mimics upon near infrared irradiation mediated photothermal therapy. J Biomed Nanotechnol 10:405–14.
[41] Incropera FP, Dewitt DP. (2001). Fundamental of heat and mass transfer, 5th edn. New York: John Wiely and Sons.
[42] ComsolMultiphysics 3.4 software.
[43] Hawkins CL, Davies MJ. (2001). Generation and propagation of radical reactions on proteins. Biochi Biophy Acta 15:196–219.
[44] Halliwell B, Gutteridge J. (1999). Free radicals in biology and medicine, Oxford: Oxford University Press.
[45] Miles CA, Bailey AJ. (1999). Thermal denaturation of collagen revisited. J Chem Sci 111:71.
[46] Bella J, Brodsky B, Berman HM. (1995). Hydration structure of a collagen peptide. Structure 15:893–906.
[47] Bozec L, Odlyha M. (2011). Thermal denaturation studies of collagen b microthermal analysis and atomic force microscopy. Biophys J 101:228–36.
[48] Miles CA, Burjanadze TV, Bailey AJ. (1995). The kinetics of the thermal denaturation of collagen in unrestrained rat tail tendon determined by differential scanning calorimetry. J Mol Biol 245:437–46.
[49] Kawahara H, Nishi KY, Nakamura S, *et al*. (2005). Effect of hydration on the stability of the collagen-like triple-helical structure of [4(R)-Hydroxyprolyl-4(R)-hydroxyl-prolylglycine]10. Biochem 44:15812–22.

[50] De Groot J. (2007). Damage assessment of parchment with scanning probe microscopy. UK: University of London.
[51] Payen K, Veis A. (1988). Fourier transform infrared spectroscopy of collagen and gelatin: deconvolution of the amide I band for conformational studies. Biopolymer 27:1749–60.
[52] Dumitrascu M, Meltzer V, Sima E, *et al*. (2011). Characterization of electron beam irradiated collagen-polyvinylpyrrolidone (PVP) and collagen-dextran (DEX) blends. J Nanomat Biostruct 6:1793.
[53] Sachlos E, Reis N, Ainsley C, *et al*. (2003). Novel collagen scaffolds with predefined internal morphology made by solid freeform fabrication. Biomaterials 24:1487–97.
[54] Hea L, Mub Shi CJ, *et al*. (2011). Modification of collagen with a natural cross-linker, procyanidin. Int J Biol Macromol 48:354–59.
[55] Kaminska A, Sionkowska A. (1996). Effect of UV radiation on the infrared spectra of collagen. Polym Degrad Stab 51:19–26.
[56] Rabotyagova OS, Cebe P, Kaplan DL. (2008). Collagen structural hierarchy and susceptibility to degradation by ultraviolet radiation. Mater Sci Eng C: Mater Biol Appl Eng 28:1420–9.
[57] Sionkowska A. (2006). Effects of solar radiation on collagen and chitosan films. J Photochem Photobiol B: Biol 82:9–15.
[58] DeCampos B, Luiza VM, Mello S. (2011). Collagen type I amide I band infrared spectroscopy. Micro 42:283–9.